Bipartite determinants mediate an evolutionarily conserved interaction between Cdc48 and the 20*S* peptidase

Dominik Barthelme and Robert T. Sauer[1]

Department of Biology, Massachusetts Institute of Technology, Cambridge, MA 02139

Contributed by Robert T. Sauer, January 8, 2013 (sent for review December 7, 2012)

Proteasomes are essential and ubiquitous ATP-dependent proteases that function in eukarya, archaea, and some bacteria. These destructive but critically important proteolytic machines use a 20*S* core peptidase and a hexameric ATPase associated with a variety of cellular activities (AAA+) unfolding ring that unfolds and spools substrates into the peptidase chamber. In archaea, 20*S* can function with the AAA+ Cdc48 or proteasome-activating nucleotidase (PAN) unfoldases. Both interactions are stabilized by C-terminal tripeptides in AAA+ subunits that dock into pockets on the 20*S* periphery. Here, we provide evidence that archaeal Cdc48 also uses a distinct set of near-axial interactions to bind 20*S* and propose that similar dual determinants mediate PAN–20*S* interactions and $Rpt_{1–6}$–20*S* interactions in the 26*S* proteasome. Current dogma holds that the $Rpt_{1–6}$ unfolding ring of the 19*S* regulatory particle is the only AAA+ partner of eukaryotic 20*S*. By contrast, we show that mammalian Cdc48, a key player in cell-cycle regulation, membrane fusion, and endoplasmic-reticulum–associated degradation, activates mammalian 20*S* and find that a mouse Cdc48 variant supports protein degradation in combination with 20*S*. Our results suggest that eukaryotic Cdc48 orthologs function directly with 20*S* to maintain intracellular protein quality control.

AAA+ protease | p97

AAA+ (ATPase associated with a variety of cellular activities) enzymes use cycles of ATP binding and hydrolysis to exert mechanical forces on substrates and power a diverse array of biological functions (1). In all cells, protein-unfolding machines of the AAA+ family form hexameric rings that cooperate with associated peptidases to execute intracellular protein degradation (2). The proteolytic sites of AAA+ proteases are sequestered within the interior of a barrel-shaped, self-compartmentalized peptidase, accessible only through narrow axial entrance tunnels that exclude folded proteins. Peptidase access is controlled by the AAA+ unfoldase, which docks with the peptidase, pulls the native structure of target proteins apart, and then translocates the polypeptide through its axial channel and into the degradation chamber.

The 20*S* peptidase is the degradation module for proteasomes in all domains of life, but functions with different AAA+ unfoldases, including the $Rpt_{1–6}$ unfolding ring of the eukaryotic 26*S* proteasome, the double-ring Cdc48 or single-ring proteasome-activating nucleotidase (PAN) enzymes in archaeal proteasomes, and the Mpa unfoldase in *Actinobacteria* (Fig. 1*A*) (3–6). In all organisms, the 20*S* peptidase has a four-ring $\alpha_7\beta_7\beta_7\alpha_7$ structure and uses N-terminal residues of the α subunits to gate entrance of substrates into its degradation chamber (Fig. 1*B*) (5, 7–9).

The subunits of the AAA+ ring have C-terminal tripeptides that dock into conserved pockets on the peptidase α ring and help stabilize an open-gate conformation to allow 20*S* degradation of proteins or large peptides (Fig. 1*B*) (10). These tripeptides generally match a hydrophobic, tyrosine, any residue motif (HbYX). Indeed, HbYX-peptidase interactions have been proposed to be both necessary and sufficient for docking and regulation (10). However, we recently discovered that the HbYX motif of archaeal Cdc48 was not essential for functional collaboration with archaeal 20*S*, suggesting that additional interactions between the AAA+ ring and 20*S* must exist (4). Eukaryotic Cdc48, which is also called p97 or valosin-containing protein (VCP), is an essential enzyme that plays roles in cell-cycle regulation, postmitotic membrane fusion, endoplasmic-reticulum-associated degradation, and the ubiquitin-proteasome system (11–13). Cdc48 is generally thought to function upstream of the 26*S* proteasome, for example by powering retro translocation of substrates across the endoplasmic reticulum membrane or disassembling macromolecular complexes (14, 15). However, Cdc48 has also been proposed to function more directly with the 26*S* proteasome (16). Despite having HbYX tails (Fig. 1*C*), eukaryotic Cdc48 has never been reported to interact directly with 20*S*.

Here, we identify residues in loops near the bottom of the axial channel of archaeal Cdc48 that appear to function in combination with HbYX interactions to mediate 20*S* binding. We also show that mouse Cdc48 interacts functionally with the cognate mouse 20*S* peptidase as well as with archaeal 20*S* and demonstrate that a variant of mouse Cdc48 collaborates with mouse or archaeal 20*S* in protein degradation. Our results deepen understanding of the functional determinants of 20*S* interactions with AAA+ unfolding rings, suggest that the use of peripheral and near-axial contacts may be a conserved feature of many AAA+ proteases, and support a potential role for Cdc48 in higher organisms in direct 20*S*-dependent protein quality control.

Results

Probing Non-HbYX Interactions Between Archaeal Cdc48 and 20*S*. Cdc48 from the archaeon *Thermoplasma acidophilum* (*ta*Cdc48) and orthologs in archaea and eukarya contain a family-specific N domain, D1 and D2 AAA+ rings, and a flexible linker that connects the D2 ring to the C-terminal HbYX motif (Fig. 1*A*). Recently, we found that a *ta*Cdc48 variant lacking the N domain and C-terminal HbYX tripeptide ($taCdc48^{\Delta N/\Delta C3}$) bound *ta*20*S* only ~25-fold less tightly than the parental $taCdc48^{\Delta N}$ enzyme, indicating that non-HbYX residues must also make significant contributions to 20*S* binding (4). To identify potential non-HbYX contacts, we built a simple model of a Cdc48–20*S* complex by initially aligning the axis of the hexameric ring of mouse Cdc48/p97 (Protein Data Bank ID code 3CF1; ~50% homology with *ta*Cdc48; ref. 13) with the axis of a heptameric α ring from the crystal structure of *T. acidophilum* 20*S* (Protein Data Bank ID code 1YAU; ref. 17). The Cdc48 ring was then moved along and rotated around the common axis until the two rings were close and the C-terminal residues of each Cdc48 subunit (the linker and HbYX motif were disordered) were close to one of the

Author contributions: D.B. designed research; D.B. performed research; D.B. and R.T.S. analyzed data; and D.B. and R.T.S. wrote the paper.

The authors declare no conflict of interest.

[1]To whom correspondence should be addressed. E-mail: bobsauer@mit.edu.

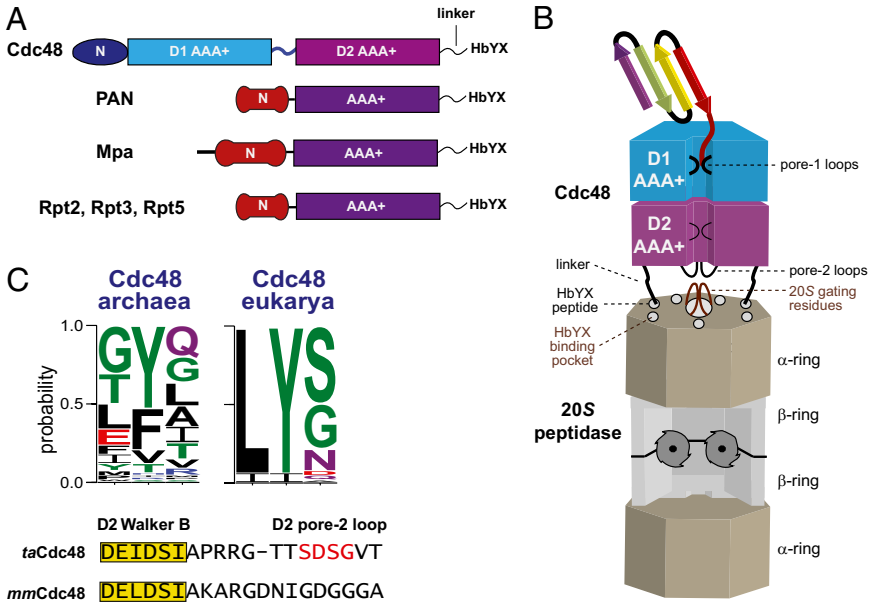

Fig. 1. Model for bipartite interactions between Cdc48 and 20*S*. (*A*) Domain architectures of the Cdc48, PAN, Mpa, and 19*S* Rpt AAA+ ATPases. Cdc48 consists of two highly homologous AAA+ domains (D1 and D2), a family-specific N-terminal domain, and a flexible and unstructured C-terminal tail consisting of a linker and the HbYX motif. Different family-specific N-domains and flexible unstructured C-termini terminating with an HbYX tripeptide are also found in the AAA+ single-ring unfoldases Mpa, PAN, and some 19*S* Rpt subunits. (*B*) Cartoon model of the archaeal Cdc48-20*S* proteasome. The N domains of Cdc48 are omitted for clarity. The HbYX tripeptides of Cdc48 dock into conserved binding pockets on the periphery of the 20*S* α ring. Near-axial interactions mediated by the pore-2 loops of the D2 ring of Cdc48 and the N-terminal gating residues of 20*S* also appear possible. (*C*) *Upper*, a WebLogo (28) representation of the C-terminal HbYX motif from archaeal and eukaryotic Cdc48. *Lower*, the sequence of pore-2 residues following the D2-ring Walker-B motif in archaeal and eukaryotic Cdc48. For functional studies, we deleted the central part of the loop (red) in archaeal Cdc48.

α-binding pockets. In this model, loops at the bottom of the axial pore of the D2 ring (pore-2 loops) were in proximity to the expected positions of N-terminal gating residues of the α ring. These potential interactions are shown in cartoon form in Fig. 1*B*. The linkers that connect the D2 ring to the HbYX docking motifs would also be in the vicinity of the α ring.

To test the importance of the linkers, we deleted the C-terminal 20 residues of *ta*Cdc48$^{\Delta N}$ (*ta*Cdc48$^{\Delta N/\Delta C20}$), which removes the HbYX motif and the complete linker region. As assayed by stimulation of peptide degradation (Fig. 2*A*), the ΔC20 deletion did not weaken *ta*20*S* binding substantially ($K_{app} = 41 \pm 8$ nM) compared with the ΔC3 deletion ($K_{app} = 24 \pm 4$ nM). However, both variants bound more weakly than the parental *ta*Cdc48$^{\Delta N}$ enzyme ($K_{app} = 2 \pm 0.5$ nM) and supported lower maximal levels of peptide degradation. By contrast, *ta*Cdc48$^{\Delta N/\Delta C20}$ and *ta*Cdc48$^{\Delta N}$ displayed similar activities in ATP hydrolysis and unfolding of GFP-ssrA in the absence of *ta*20*S* (Fig. 2*B*). *ta*Cdc48$^{\Delta N/\Delta C20}$ also supported *ta*20*S* degradation of GFP-ssrA (Fig. 2*A*, *Inset*; Fig. 2*B*). We conclude that linker residues do not make major non-HbYX interactions with archaeal 20*S* or play roles in ATP-dependent protein unfolding or translocation.

To test the importance of the D2 pore-2 loop of *ta*CDC48, we deleted the central amino acids (residues 580–583) of this loop. The *ta*Cdc48$^{\Delta N/\Delta 580-583}$ mutant displayed ~10-fold lower *ta*20*S* affinity (~20 nM) than the *ta*Cdc48$^{\Delta N}$ parent, as assayed by stimulation of peptide cleavage (Fig. 2*C*). Strikingly, although *ta*Cdc48$^{\Delta N/\Delta 580-583}$ and *ta*Cdc48$^{\Delta N/\Delta C3}$ both interacted with 20*S* with interaction constants of ~20 nM, combining the Δ580–583 and ΔC3 mutations resulted in a variant (*ta*Cdc48$^{\Delta N/\Delta 580-583/\Delta C3}$) that displayed no activation of *ta*20*S* peptide cleavage at concentrations up to 1 μM (Fig. 2*C*). These results suggest that the pore-2 loops of the D2 ring and the HbYX motifs make independent contributions to *ta*20*S* recognition. One caveat is that *ta*Cdc48$^{\Delta N/\Delta 580-583}$ and *ta*Cdc48$^{\Delta N/\Delta 580-583/\Delta C3}$ had reduced ATPase activity compared with the parental enzyme (Fig. 2*B*). Although this phenotype could reflect changes in protein conformation and thus be an indirect effect on 20*S* binding, several observations favor direct effects. First, ATP hydrolysis is not required for the interaction of *ta*Cdc48$^{\Delta N}$ with *ta*20*S* (4). Second, *ta*Cdc48$^{\Delta N/\Delta 580-583}$ fully activated peptide cleavage by *ta*20*S* (Fig. 2*C*). Third, *ta*Cdc48$^{\Delta N/\Delta 580-583}$ and *ta*Cdc48$^{\Delta N/\Delta 580-583/\Delta C3}$ had protein-unfolding activity commensurate with their reduced ATP hydrolysis activities (Fig. 2*B*) and thus are functional enzymes. Fourth, although *ta*Cdc48$^{\Delta N/\Delta 580-583}$ unfolded GFP-ssrA at ~20% of the parental rate, it supported 20*S* degradation of GFP-ssrA at only ~5% of the parental rate (Fig. 2*B*), indicating a substantially larger defect in coordination of 20*S* protein degradation than in protein unfolding.

In our model of the complex, the pore-2 loops of the D2 ring of Cdc48 were close to the expected positions of the N-terminal gating residues of the 20*S* α subunits (Fig. 1*B*). If these regions of Cdc48 and 20*S* do contact each other, then gating-residue mutations should also diminish binding. Indeed, when we deleted the gating residues in the *ta*20*S*$^{\Delta\alpha 2-12}$ mutant, higher concentrations of this enzyme were required to support GFP-ssrA degradation by a fixed concentration of *ta*Cdc48$^{\Delta N}$ in comparison with degradation by *ta*20*S* (Fig. 2*D*). This result supports a role for the near-axial gating residues of the α ring in binding Cdc48.

Evidence for Non-HbYX Recognition of 20*S* by PAN. Given our Cdc48 results, we wondered if non-HbYX interactions might also contribute to PAN–20*S* recognition. Although we previously failed to detect an interaction between a *Methanocaldococcus jannaschii* PAN variant missing the HbYX motif (*mj*PAN$^{\Delta C3}$) and *ta*20*S* (4), replacing ATP with ATPγS in the peptide-cleavage assay allowed *mj*PAN$^{\Delta C3}$ to stimulate *ta*20*S* activity with an apparent affinity of 3.8 ± 1 μM (Fig. 2*E*). Wild-type *mj*PAN bound *ta*20*S* more tightly (54 ± 7 nM) under the same conditions (Fig. 2*E*). Thus, the PAN HbYX motif makes significant contributions to 20*S* binding but is not necessary for recognition. Pore-2 loops similar

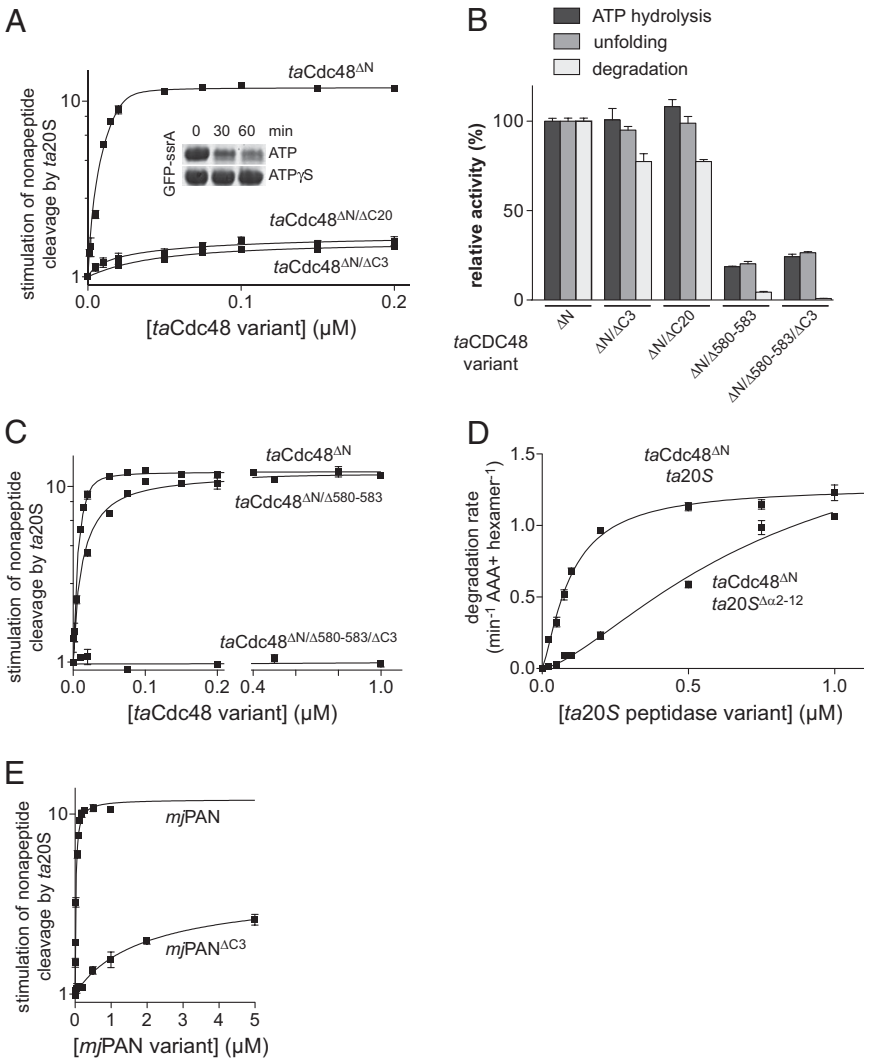

Fig. 2. AAA+ D2 pore loops contribute to 20*S* binding. (*A*) Nonapeptide cleavage by *ta*20*S* peptidase (10 nM) as a function of increasing concentrations of *ta*Cdc48 variants. Solid lines are fits to a quadratic equation for near-stoichiometric binding. Values are averages (n = 3) ± SEM. Fitted K_{app} values for *ta*Cdc48$^{\Delta N}$, *ta*Cdc48$^{\Delta N/\Delta C3}$, and *ta*Cdc48$^{\Delta N/\Delta C20}$ were 2 ± 0.5, 24 ± 4, and 42 ± 8 nM, respectively. The inset shows an SDS/PAGE assay of GFP-ssrA (5 μM) degradation by 1.2 μM *ta*Cdc48$^{\Delta N/\Delta C20}$ and 0.4 μM *ta*20*S*. Reactions were performed in the presence of 2 mM ATP and an ATP regeneration system or in the presence of 2 mM ATPγS. (*B*) ATP-hydrolysis rates, GFP-ssrA unfolding rates, and GFP-ssrA degradation rates are plotted for *ta*Cdc48 variants relative to these activities for *ta*Cdc48$^{\Delta N}$. ATP hydrolysis was measured at 45 °C in the presence of an ATP regeneration system and 2 mM ATP. Unfolding of GFP-ssrA (5 μM) by *ta*Cdc48$^{\Delta N}$ variants (0.3 μM) was assayed at 60 °C in the presence of 10 mM ATP. Degradation of GFP-ssrA (5 μM) by *ta*Cdc48$^{\Delta N}$ variants (0.3 μM) and *ta*20*S* (0.9 μM) was measured at 45 °C in the presence of 5 mM ATP and an ATP regeneration system. Values are plotted as averages (n = 3) ± SEM. (*C*) Nonapeptide cleavage by *ta*20*S* as a function of increasing concentrations of *ta*Cdc48$^{\Delta N}$ variants. Experiments were performed and analyzed as described in (*A*). For *ta*Cdc48$^{\Delta N/\Delta 580-583}$, the fitted K_{app} was 24 ± 4 nM. (*D*) Degradation of GFP-ssrA (5 μM) at 45 °C was assayed by changes in fluorescence in the presence of *ta*Cdc48$^{\Delta N}$ (50 nM) and increasing concentrations of *ta*20*S* or *ta*20*S*$^{\Delta\alpha 2-12}$. Values are averages (n = 3) ± SEM. (*E*) Nonapeptide cleavage by *ta*20*S* (10 nM) was assayed at 45 °C as a function of increasing concentrations of *mj*PAN or *mj*PAN$^{\Delta C3}$ in the presence of 100 μM ATPγS. Solid lines are fits to a quadratic equation for near-stoichiometric binding for *mj*PAN (K_{app} 54 ± 7 nM) and to a hyperbolic equation for *mj*PAN$^{\Delta C3}$ (K_{app} 3.8 ± 1 μM). Values are averages (n = 3) ± SEM.

to those in the D2 ring of Cdc48 are also present in the single AAA+ rings of PAN, Mpa, and the Rpt_{1-6} subunits of the 26*S* proteasome (18), raising the possibility that all of these enzymes use a combination of peripheral HbYX contacts and near-axial interactions to collaborate with the 20*S* peptidase.

Eukaryotic 20*S* Interacts Functionally with Cdc48. In eukaryotes, both the α_7 and β_7 rings of 20*S* consist of seven genetically distinct subunits, whereas the corresponding rings in archaeal 20*S* are each built from seven identical subunits (5). Moreover, in the 26*S* proteasome, the C-terminal tails of the Rpt_{1-6} subunits in the AAA+ unfolding ring differ in sequence and dock with distinct α subunits in the 20*S* core peptidase (10, 19–21). Did evolution of eukaryotic 20*S* result in loss of functional interactions with Cdc48? To address this question, we initially used *Saccharomyces cerevisiae* 20*S* (*sc*20*S*) and tested if archaeal *ta*Cdc48 or *ta*Cdc48$^{\Delta N}$ could stimulate peptide cleavage. Indeed, both *ta*Cdc48 enzymes enhanced peptide cleavage by yeast *sc*20*S* (Fig. 3*A*). Moreover, robust degradation of GFP-ssrA was observed when we combined *ta*Cdc48$^{\Delta N}$ and *sc*20*S* (Fig. 3*B*). Thus, a homomeric Cdc48 AAA+ ring can functionally collaborate with the heteromeric rings of yeast 20*S* both in gate opening and protein degradation.

Next, we tested if eukaryotic Cdc48, which harbors conserved 20*S* binding motifs (Fig. 1*C*), could functionally interact with 20*S*, either from the same eukaryotic species or from archaea.

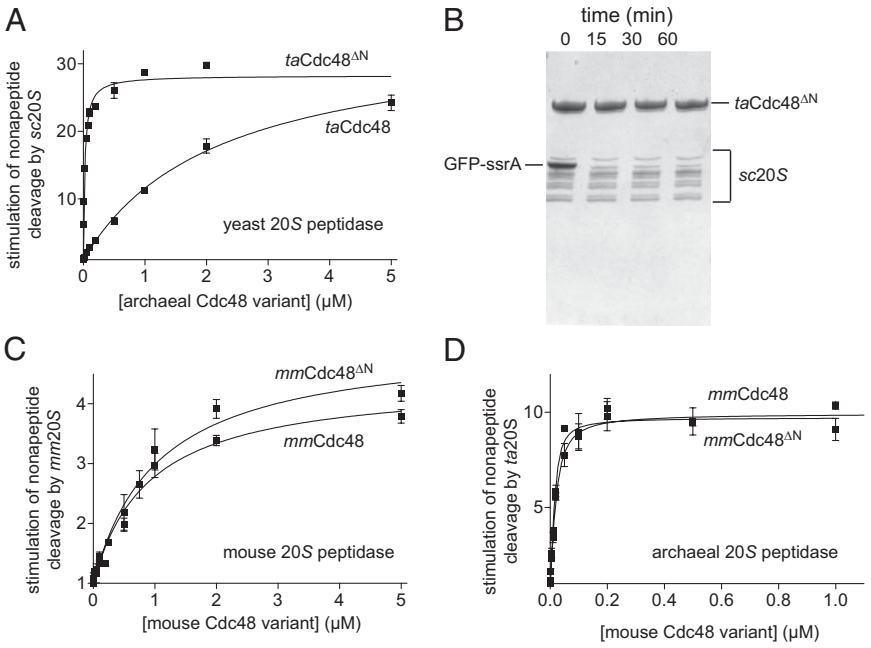

Fig. 3. Evolutionary conservation of a direct Cdc48–20*S* interaction. (*A*) Nonapeptide cleavage by the *S. cerevisiae* 20*S* peptidase (10 nM) as a function of increasing concentrations of *ta*Cdc48 or *ta*Cdc48$^{\Delta N}$. Experiments were performed at 37 °C in the presence of 2 mM ATP. Data were fit to a hyperbolic equation for *ta*Cdc48 (K_{app} 2.2 ± 0.2 μM) or a quadratic equation for near stoichiometric binding for *ta*Cdc48$^{\Delta N}$ (K_{app} 24 ± 2 nM). Values are averages (n = 3) ± SEM. (*B*) SDS/PAGE assay of GFP-ssrA (5 μM) degradation by *ta*Cdc48$^{\Delta N}$ (1.2 μM) and *sc*20*S* (0.4 μM). Reactions were performed at 37 °C in the presence of 2 mM ATP and an ATP regeneration system. (*C*) Stimulation of nonapeptide cleavage by mouse 20*S* (5 nM) was assayed at 37 °C in the presence of 100 μM ATPγS and increasing concentrations of mouse Cdc48 or mouse Cdc48$^{\Delta N}$. The lines are fits to a hyperbolic equation with K_{app} values of 0.9 ± 0.2 μM (*mm*Cdc48) and 1.0 ± 0.2 μM (*mm*Cdc48$^{\Delta N}$). Values are averages (n = 3) ± SEM. (*D*) Stimulation of nonapeptide cleavage by archaeal *ta*20*S* peptidase (10 nM) by increasing concentrations of mouse Cdc48 or mouse Cdc48$^{\Delta N}$. The lines are fits to a quadratic equation for near stoichiometric binding with K_{app} values of 10 ± 2 nM (*mm*Cdc48) and 5 ± 2 nM (*mm*Cdc48$^{\Delta N}$). Experiments were performed at 37 °C in the presence of ATP (2 mM).

For these experiments, we used mouse Cdc48 and an ΔN variant of this enzyme, because these *Mus musculus* enzymes (*mm*Cdc48 and *mm*Cdc48$^{\Delta N}$) were better behaved than the comparable yeast enzymes. Importantly, *mm*Cdc48 and *mm*Cdc48$^{\Delta N}$ enhanced peptide cleavage by mouse 20*S* (Fig. 3*C*). The *mm*Cdc48 and *mm*Cdc48$^{\Delta N}$ enzymes also stimulated peptide cleavage by archaeal *ta*20*S* (Fig. 3*D*). Thus, mouse Cdc48 interacts both with mouse 20*S* and with the archaeal homolog of this enzyme. Binding of *mm*Cdc48 to mouse 20*S* (K_{app} ~1 μM) was weaker than binding to *ta*20*S* (K_{app} ~10 nM), and the ΔN deletion in mouse Cdc48 did not strengthen 20*S* affinity as it does in archaeal Cdc48. Nevertheless, mammalian Cdc48 retains the ability to interact functionally with mammalian 20*S*.

20*S*-Dependent Degradation by an Altered-Specificity Mouse Cdc48 Variant. GFP-ssrA is recognized and unfolded by archaeal Cdc48 but not by mouse Cdc48 (22). However, Zwickl and colleagues showed that substituting a Tyr-Tyr (YY) sequence from the D1 pore-1 loop of *ta*Cdc48 for the corresponding Leu-Ala (LA) sequence in mouse Cdc48$^{\Delta N}$ transplanted the ability to recognize and unfold GFP-ssrA (22). We found that *mm*Cdc48$^{YY/\Delta N}$ was able to collaborate with both *mm*20*S* and *ta*20*S* to degrade GFP-ssrA (Fig. 4 *A* and *B*). No degradation was observed without *mm*Cdc48$^{YY/\Delta N}$, without ATP, or when MG132, a 20*S* peptidase inhibitor, was added. For *mm*Cdc48$^{YY/\Delta N}$–*ta*20*S*, V_{max} and K_M for GFP-ssrA degradation (Fig. 4*C*) were similar to values for *ta*Cdc48$^{\Delta N}$–*ta*20*S* degradation of this substrate (4). Thus, the enzymatic machinery required for protein degradation is still present, at least vestigially, in mammalian Cdc48.

We did not detect GFP-ssrA degradation by *mm*Cdc48 or *mm*Cdc48^{YY} in the presence of *ta*20*S* (Fig. 4*D*). Thus, the N domain of *mm*Cdc48 represses unfolding/degradation, as we previously observed for the N domain of archaeal *ta*Cdc48 (4). The structure of the N domain is similar but not identical in archaeal and mammalian Cdc48, but the N-domain sequence is relatively poorly conserved between archaea and eukarya. These variations probably account for the differences observed in N-domain modulation of the activity of the archaeal and mammalian enzymes.

Discussion

Attempts to detect functional interactions between eukaryotic Cdc48 and 20*S* have not previously been successful (23). For example, it was recently noted that no eukaryotic Cdc48–20*S* complex has been isolated or successfully reconstituted (24). We revisited this issue because archaeal Cdc48 and 20*S* comprise a functional proteasome, and the archaeal and eukaryotic orthologs of these enzymes share substantial sequence and structural homology (4). Our current biochemical results demonstrate functional collaboration between the Cdc48 and 20*S* enzymes from mouse and also show that eukaryotic 20*S* can function with archaeal Cdc48 and vice versa. Based on these results, we propose that eukaryotic 20*S* could be a component of a Cdc48–20*S* complex as an alternative to binding the 19*S* regulatory particle to form the 26*S* proteasome.

Whether a eukaryotic Cdc48–20*S* complex functions as an alternative proteasome remains to be determined but mouse Cdc48 can clearly function as a 20*S* activator. In addition, our studies show that mouse Cdc48 variants contain the machinery needed to unfold and translocate protein substrates into the 20*S* degradation chamber. Moreover, degradation by mouse 20*S* and a Cdc48 variant was inhibited by MG132. Thus, if Cdc48–20*S* did function as an alternative eukaryotic proteasome, then inhibition of substrate proteolysis by MG132 or related 20*S* inhibitors would not be sufficient to distinguish between degradation by the 26*S* proteasome or Cdc48–20*S*. The role of

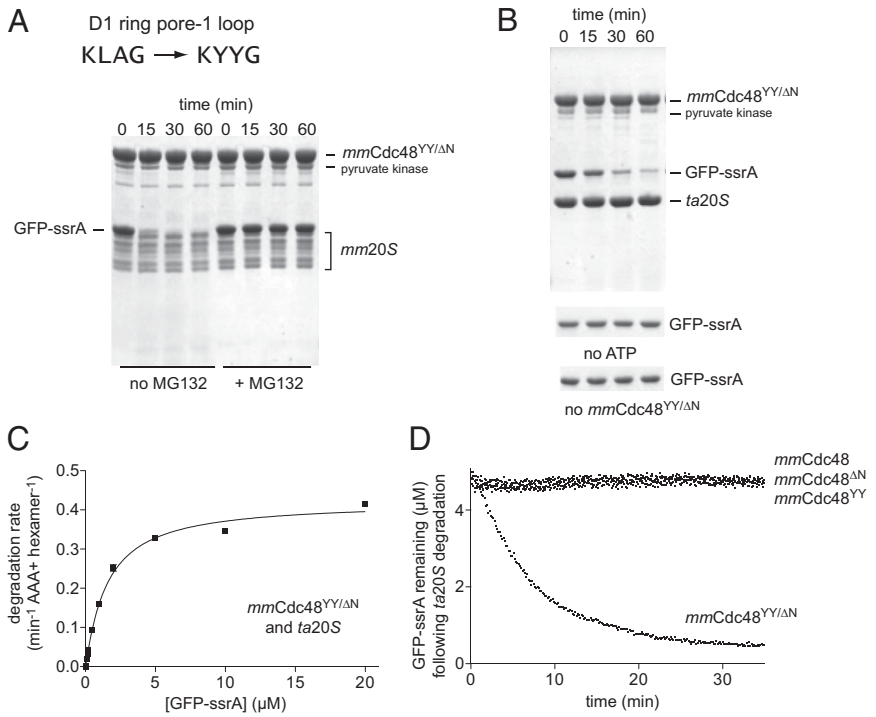

Fig. 4. Protein degradation by mouse 20*S* and a mouse Cdc48 variant. (*A*) In the *mm*Cdc48$^{YY/\Delta N}$ variant of mouse Cdc48, the pore-1 loop of the D1 ring is mutated from KLAG to KYYG to match the sequence in *ta*Cdc48. The gel shows an SDS/PAGE assay of degradation of GFP-ssrA (5 μM) by *mm*Cdc48$^{YY/\Delta N}$ (1.2 μM) and *mm*20*S* (0.4 μM) at 37 °C with 2 mM ATP and a pyruvate-kinase based ATP regeneration system. Degradation was inhibited by MG132 (100 μM). (*B*) SDS/PAGE assay of GFP-ssrA degradation by *mm*Cdc48$^{YY/\Delta N}$ and *ta*20*S* using the same conditions as in (*A*). The gel strips on the bottom show that GFP-ssrA is not degraded without ATP or without *mm*Cdc48$^{YY/\Delta N}$. (*C*) Michaelis-Menten plots of the steady-state degradation of different concentrations of GFP-ssrA by *ta*20*S* (0.9 μM) and *mm*Cdc48$^{YY/\Delta N}$ (0.3 μM). The fitted K_M was 1.7 ± 0.1 μM and V_{max} was 0.43 ± 0.01 min^{-1} Cdc48$_6^{-1}$. (*D*) As assayed by loss of native fluorescence, GFP-ssrA (5 μM) was not degraded by *ta*20*S* (0.4 μM) in the presence of *mm*Cdc48, *mm*Cdc48$^{\Delta N}$, or *mm*Cdc48^{YY} (1.2 μM) but was degraded when *mm*Cdc48$^{YY/\Delta N}$ (1.2 μM) was present.

Cdc48 in eukaryotic protein degradation has generally been thought to involve extracting proteins from membranes or macromolecular complexes for delivery to the 26*S* proteasome, although some studies suggest that Cdc48 works more directly with 26*S* (14–16). Indirect roles of Cdc48, direct roles in collaboration with the 26*S* proteasome, and direct roles of a Cdc48–20*S* proteasome all remain possible. The challenge will be to identify substrates degraded by one or more of these Cdc48-dependent mechanisms.

Docking of C-terminal HbYX tripeptides into pockets on the periphery of the 20*S* α ring are important for 20*S* binding by archaeal PAN and the Rpt$_{1–6}$ unfolding ring of the 19*S* eukaryotic regulatory particle (10, 19, 21). HbYX-α interactions also help stabilize binding of Cdc48 to 20*S*, but archaeal Cdc48 still binds and functionally collaborates with 20*S* after deletion of this C-terminal tripeptide (4). Our current results show that PAN lacking the HbYX motif also binds archaeal 20*S* and stimulates peptide cleavage. We also found that near-axial interactions mediated by residues in the pore-2 loop in the Cdc48 D2 ring, which are positioned to interact with N-terminal gating residues of the α subunits, appear to stabilize functional complexes between Cdc48 and 20*S*. Based on sequence and architectural homology, similar interactions may help stabilize Mpa–20*S*, PAN–20*S*, and 19*S*–20*S* binding. Thus, 20*S* binding by the AAA + rings of Mpa, Cdc48, PAN, and Rpt$_{1–6}$ may all involve peripheral HbYX-α contacts as well as near-axial contacts between N-terminal α gating residues and pore-2 residues in the AAA+ rings. Interestingly, the length of the pre-HbYX linker varies significantly between archaeal Cdc48 (~1–19 residues) and eukaryotic Cdc48 (~29–47 residues). Nevertheless, we find that archaeal 20*S* functionally interacts with eukaryotic Cdc48 and vice versa. Near-axial interactions may help to make these interactions between enzymes from different domains of life possible despite the observed linker-length differences. Whether the longer linkers of eukaryotic Cdc48 are important for other functions, such as interactions with specific adaptors, remains to be determined.

The hexameric AAA+ ring of the ClpX unfoldase also interacts with the heptameric rings of the ClpP peptidase, which is structurally unrelated to 20*S*, using peripheral contacts as well as near-axial interactions between pore-2 loops in the ClpX ring and N-terminal residues that surround the entry pore to the ClpP chamber (25). For ClpXP, these near-axial interactions vary dynamically with nucleotide state, help control the rate of ATP hydrolysis, and facilitate efficient protein unfolding (25). Thus, bipartite interactions between AAA+ unfoldases and their cognate peptidases may be common features of many AAA+ proteases. Near-axial contacts may coordinate substrate translocation through the central pore of the unfoldase ring and into the degradation chamber of the peptidase. Crystal structures of 20*S* with the heptameric ATP-independent activator PA26 also show peripheral interactions between C-terminal tails and pockets in the α ring as well as interactions between an internal activation loop in PA26 and the near-axial gating residues of the α ring (17), further supporting the possibility that bipartite recognition is a universal feature of functional interactions with the 20*S* peptidase.

Materials and Methods

Plasmids and Strains. The mouse Cdc48 gene was amplified from *Mus musculus* cDNA by PCR and cloned into the pET28A (NdeI/SalI) expression vector, resulting in fusion of an N-terminal His$_6$-thrombin tag to Cdc48. Mutations

were generated by site-directed mutagenesis and verified by sequencing. The *S. cerevisiae* strain RJD1144 [*MAT*a, *his3Δ200 leu2-3,112 lys2-801 trpΔ63 ura3-52 PRE1-FLAG-6xHIS::Ylplac211* (*URA3*)] was generously provided by R. Deshaies (California Institute of Technology, Pasadena, CA)].

Expression and Protein Purification. The *ta*Cdc48, *ta*20*S*, *mj*PAN, and GFP-ssrA proteins were expressed and purified as described (4). *mm*Cdc48 proteins were expressed in strain *Escherichia coli* BL21 (DE3) RIL (Stratagene). Protein expression was induced at OD_{600} ~0.8 by adding 1 mM isopropyl β-D-1-thiogalactopyranoside, and growing cells for an additional 4 h at 37 °C. Cells were harvested by centrifugation, resuspended in 50 mM Hepes·KOH (pH 7.5), 50 mM NaCl, 5 mM $MgCl_2$, 0.5 mM EDTA, and 1 mM DTT in the presence of a protease inhibitor mix (Roche), 1,000 units Benzonase (Sigma-Aldrich), and 1 mg/mL lysozyme, and lysed by sonication. Cellular debris were removed by centrifugation at 30,000 × *g* for 30 min. Polyethylenimine (0.1% vol/vol) was added to the supernatant to precipitate nucleic acids, which were removed by a centrifugation at 30,000 × *g* for 30 min. The cleared supernatant was incubated with washed Ni^{++}-NTA beads (Thermo Scientific) at 4 °C for 2 h. After washing with 50 mM NaH_2PO_4 (pH 8.0), 500 mM KCl, 50 mM imidazole, and 0.5 mM EDTA, proteins were eluted with 500 mM imidazole. Samples were dialyzed against 20 mM Tris·HCl (pH 8.0), 50 mM NaCl, 1 mM DTT, and 1 mM EDTA and loaded onto a MonoQ column (GE Healthcare) followed by elution with a linear salt gradient from 50 mM to 1 M NaCl. After thrombin cleavage overnight, fractions containing Cdc48 were loaded onto a Superdex 200 (16/60) column (GE Healthcare) equilibrated in 50 mM Hepes·KOH (pH 7.5), 100 mM NaCl, 1 mM EDTA, and 1 mM DTT. Cdc48 fractions that eluted at a position expected for hexamers were concentrated and frozen in liquid nitrogen for storage at –80 °C.

The yeast 20*S* core peptidase was isolated from *S. cerevisiae* strain RJD1144, which contains a Flag-His_6 tag on Pre1, using anti-FLAG M2 resin (Sigma-Aldrich) and size-exclusion chromatography as described (26, 27). Mouse 20*S* peptidase was purchased from R&D Systems. Cdc48 and PAN concentrations are reported as hexamer equivalents. 20*S* concentrations are reported as $\alpha_7\beta_7\beta_7\alpha_7$ equivalents.

Peptidase Assays. Cleavage of Mca-AKVYPYPME-Dpa(Dnp)-amide by *ta*20*S* in the presence or the absence of *ta*Cdc48 was assayed at 45 °C as described (4). For reactions containing *mm*Cdc48 variants, the assay temperature was 37 °C. Cleavage of Mca-RPPGFSAFK-(Dnp)-OH (R&D Systems) by *mm*20*S* (5 nM) was measured in the presence or absence of *mm*Cdc48 or *ta*Cdc48 at 37 °C. Reactions were performed in 50 μL R buffer (25 mM Hepes·KOH, pH 7.5, 50 mM potassium acetate, and 5 mM magnesium acetate) and assayed by changes in fluorescence (excitation 340 nm; emission 405 nm) using a Spectramax 5 spectrofluorometer (Molecular Devices). Cleavage of Mca-RPPGFSAFK-(Dnp)-OH by *sc*20*S* (10 nM) was assayed at 37 °C in R buffer plus 0.01% (vol/vol) IGEPAL CA-630.

Protein Unfolding and Degradation Assays. Protein unfolding was assayed by loss of GFP-ssrA fluorescence (excitation 467 nm; emission 511 nm) in a Spectramax 5 plate reader (Molecular Devices). Reactions were performed in 30 μL 50 mM Hepes·KOH (pH 7.5), 100 mM KCl, and 20 mM $MgCl_2$ at 60 °C for *ta*Cdc48 and 37 °C for *mm*Cdc48 variants. Reaction components were preincubated for 20 min before adding 10 mM ATP. Protein degradation was assayed by loss of GFP-ssrA fluorescence and SDS/PAGE at 37 °C for *mm*Cdc48 variants, 20*S* or at 45 °C for *ta*Cdc48 and 20*S* peptidase in 30 μL 50 mM Tris·HCl (pH 8.0), 100 mM NaCl, 20 mM $MgCl_2$, 3% (vol/vol) glycerol, 5 mM ATP, and an ATP-regenerating system (20 $U{\cdot}mL^{-1}$ pyruvate kinase; 15 mM phosphoenolpyruvate).

ACKNOWLEDGMENTS. We thank R. Deshaies for generously providing the *S. cerevisiae* strains. Supported by National Institutes of Health Grant AI-16892.

1. Hanson PI, Whiteheart SW (2005) AAA+ proteins: Have engine, will work. *Nat Rev Mol Cell Biol* 6(7):519–529.
2. Sauer RT, Baker TA (2011) AAA+ proteases: ATP-fueled machines of protein destruction. *Annu Rev Biochem* 80:587–612.
3. Smith DM, et al. (2005) ATP binding to PAN or the 26S ATPases causes association with the 20S proteasome, gate opening, and translocation of unfolded proteins. *Mol Cell* 20(5):687–698.
4. Barthelme D, Sauer RT (2012) Identification of the Cdc48·20*S* proteasome as an ancient AAA+ proteolytic machine. *Science* 337(6096):843–846.
5. Voges D, Zwickl P, Baumeister W (1999) The 26S proteasome: A molecular machine designed for controlled proteolysis. *Annu Rev Biochem* 68:1015–1068.
6. Wang T, et al. (2009) Structural insights on the *Mycobacterium tuberculosis* proteasomal ATPase Mpa. *Structure* 17(10):1377–1385.
7. Groll M, et al. (2000) A gated channel into the proteasome core particle. *Nat Struct Biol* 7(11):1062–1067.
8. Löwe J, et al. (1995) Crystal structure of the 20*S* proteasome from the archaeon *T. acidophilum* at 3.4 A resolution. *Science* 268(5210):533–539.
9. Stadtmueller BM, Hill CP (2011) Proteasome activators. *Mol Cell* 41(1):8–19.
10. Smith DM, et al. (2007) Docking of the proteasomal ATPases' carboxyl termini in the 20*S* proteasome's alpha ring opens the gate for substrate entry. *Mol Cell* 27(5): 731–744.
11. Meyer H, Bug M, Bremer S (2012) Emerging functions of the VCP/p97 AAA-ATPase in the ubiquitin system. *Nat Cell Biol* 14(2):117–123.
12. Hirsch C, Gauss R, Horn SC, Neuber O, Sommer T (2009) The ubiquitylation machinery of the endoplasmic reticulum. *Nature* 458(7237):453–460.
13. Davies JM, Brunger AT, Weis WI (2008) Improved structures of full-length p97, an AAA ATPase: Implications for mechanisms of nucleotide-dependent conformational change. *Structure* 16(5):715–726.
14. Braun S, Matuschewski K, Rape M, Thoms S, Jentsch S (2002) Role of the ubiquitin-selective CDC48(UFD1/NPL4) chaperone (segregase) in ERAD of OLE1 and other substrates. *EMBO J* 21(4):615–621.
15. Rape M, et al. (2001) Mobilization of processed, membrane-tethered SPT23 transcription factor by CDC48(UFD1/NPL4), a ubiquitin-selective chaperone. *Cell* 107(5): 667–677.
16. Verma R, Oania R, Fang R, Smith GT, Deshaies RJ (2011) Cdc48/p97 mediates UV-dependent turnover of RNA Pol II. *Mol Cell* 41(1):82–92.
17. Förster A, Masters EI, Whitby FG, Robinson H, Hill CP (2005) The 1.9 A structure of a proteasome-11S activator complex and implications for proteasome-PAN/PA700 interactions. *Mol Cell* 18(5):589–599.
18. Zhang F, et al. (2009) Structural insights into the regulatory particle of the proteasome from Methanocaldococcus jannaschii. *Mol Cell* 34(4):473–484.
19. Kumar B, Kim YC, DeMartino GN (2010) The C terminus of Rpt3, an ATPase subunit of PA700 (19 S) regulatory complex, is essential for 26 S proteasome assembly but not for activation. *J Biol Chem* 285(50):39523–39535.
20. Rabl J, et al. (2008) Mechanism of gate opening in the 20*S* proteasome by the proteasomal ATPases. *Mol Cell* 30(3):360–368.
21. Tian G, et al. (2011) An asymmetric interface between the regulatory and core particles of the proteasome. *Nat Struct Mol Biol* 18(11):1259–1267.
22. Rothballer A, Tzvetkov N, Zwickl P (2007) Mutations in p97/VCP induce unfolding activity. *FEBS Lett* 581(6):1197–1201.
23. Isakov E, Stanhill A (2011) Stalled proteasomes are directly relieved by P97 recruitment. *J Biol Chem* 286(35):30274–30283.
24. Matouschek A, Finley D (2012) Cell biology. An ancient portal to proteolysis. *Science* 337(6096):813–814.
25. Martin A, Baker TA, Sauer RT (2007) Distinct static and dynamic interactions control ATPase-peptidase communication in a AAA+ protease. *Mol Cell* 27(1):41–52.
26. Lander GC, et al. (2012) Complete subunit architecture of the proteasome regulatory particle. *Nature* 482(7384):186–191.
27. Verma R, et al. (2000) Proteasomal proteomics: Identification of nucleotide-sensitive proteasome-interacting proteins by mass spectrometric analysis of affinity-purified proteasomes. *Mol Biol Cell* 11(10):3425–3439.
28. Crooks GE, Hon G, Chandonia JM, Brenner SE (2004) WebLogo: A sequence logo generator. *Genome Res* 14(6):1188–1190.